Ecological Indicators 151 (2023) 110326

Contents lists available at ScienceDirect

Ecological Indicators

journal homepage: www.elsevier.com/locate/ecolind

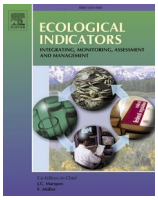

Climate warming-induced phenology changes dominate vegetation productivity in Northern Hemisphere ecosystems

Chaoya Dang [a], Zhenfeng Shao [a,*], Xiao Huang [b], Qingwei Zhuang [a], Gui Cheng [a], Jiaxin Qian [a]

[a] The State Key Laboratory of Information Engineering in Surveying, Mapping and Remote Sensing, Wuhan University, Wuhan 430079, China
[b] Department of Geosciences, University of Arkansas, Fayetteville, AR 72701, USA

ARTICLE INFO

Keywords:
Ecosystem productivity
Vegetation phenology
Soil moisture
Temperature
Dominant factor
Climate change

ABSTRACT

The climate change is expected to trigger changes in vegetation phenology, temperature, and soil moisture (SM), altering the productivity of ecosystems. Despite numerous existing efforts, however, their contradicting conclusions suggest that how vegetation productivity is impacted by these factors still remains unclear in the Northern Hemisphere ecosystems (≥25°N). This study used the optimal fingerprint (OFP) method and redundancy analysis (RDA) to attribute the importance of key drivers of vegetation productivity from 2001 to 2019 based on long-term remote sensing and FLUXNET observation data. The results showed that solar-induced chlorophyll fluorescence (SIF), gross primary productivity (GPP), and net primary productivity (NPP) were increased in 72.01% to 88.04% of the vegetation areas. We observed that the correlation between vegetation productivity and spring phenology, autumn phenology, growing season length (GSL), SM, temperature reached 99% significance level, where early spring phenology, delayed autumn phenology, extended GSL, increased SM, and elevated temperature all enhanced ecosystem productivity, with GSL being the most important factor driving vegetation productivity. In addition, the pixel-wise attribution analysis indicated that GSL, as the dominant driver, accounted for 30.24% of the vegetation productivity, followed by temperature (23.79%), spring phenology (19.56%), autumn phenology (14.09%), and SM (12.31%), all of which were dominated by positive effects (54.19% to 73.14%). The results from this study serve as important references that benefit our understanding of driving mechanisms of temperature-phenology-SM interactions on ecosystem productivity.

1. Introduction

Vegetation photosynthesis regulates 90% of the global gas exchange between the terrestrial biosphere and the atmosphere, where gross primary productivity (GPP) is the largest global carbon flux and a key parameter for quantifying ecosystem carbon sequestration capacity (Goetz and Prince, 1999). The terrestrial ecosystems at middle and high latitudes play an important role in regulating the global carbon cycle and atmospheric CO_2 concentration (Braswell et al., 1997; Piao et al., 2008; Jia and Zhou, 2023). Therefore, it is important to accurately understand the dominant drivers of vegetation productivity at middle and high latitude ecosystems in the Northern Hemisphere.

Under the context of global climate change, scholars have observed notable changes in meteorological and hydrological (e.g., temperature and soil moisture (SM)) conditions (IPCC, 2013; Albergel et al., 2013; Deng et al., 2020). One of the main controls of phenology is the temperature (Walther et al., 2002; Keenan et al., 2014; Fu et al., 2015), with warming temperatures advancing spring phenology (hereinafter referred to as SOS), delaying autumn phenology (hereinafter referred to as EOS) (Menzel et al., 2006; Körner and Basler, 2010), and extending growing season length (GSL). Studies have shown that the extension of the vegetation GSL leads to an increase in vegetation productivity (Richardson et al., 2010; Dragoni et al., 2011; Keenan et al., 2014; Gonsamo et al., 2017). However, other studies found contradicting evidence (Piao et al., 2008; Barichivich et al., 2013). Therefore, it remains unclear what role vegetation phenology changes play in driving vegetation productivity in terrestrial ecosystems.

In addition, there are many factors directly and indirectly affecting vegetation productivity. Increasing CO_2 concentrations drive enhanced vegetation productivity (Wang et al., 2020) and also lead to rising temperatures (Came et al., 2007). With continued warming, radiation limitation will increase and impose a strong upper limit on boreal ecosystem productivity (Zhang et al., 2020). Nutrient availability determines potential vegetation productivity, and actual productivity

* Corresponding author.
E-mail address: shaozhenfeng@whu.edu.cn (Z. Shao).

https://doi.org/10.1016/j.ecolind.2023.110326
Received 2 February 2023; Received in revised form 10 April 2023; Accepted 2 May 2023
Available online 7 May 2023

depends on nutrient recycling (Vergutz et al., 2012; Scalon et al., 2022). Moreover, many pieces of evidence suggest that variations in temperatures and SM affect the vegetation productivity (Green et al., 2019; Nemani et al., 2003; Huang et al., 2019; Liu et al., 2020a; Dang et al., 2022; dela Torre et al., 2021). For future projections, studies have shown an increasing trend in temperatures (IPCC, 2013) while a decreasing trend in SM (Albergel et al., 2013; Deng et al., 2020). In terms of temperature, ecosystems in the Northern Hemisphere ecosystems have not yet reached optimal photosynthetic temperatures (Huang et al., 2019), and rising temperatures is expected to continue boosting vegetation productivity. However, increased temperatures can lead to higher vapor pressure deficit (VPD), resulting in vegetation stomatal closure (Williams et al., 2012) and increased vegetation transpiration (Liu et al., 2020b), which in turn limits vegetation productivity (He et al., 2022). The changes in SM can also greatly alter vegetation productivity (Green et al., 2019; Liu et al., 2020a; Wu et al., 2021). Studies have shown that reduced SM in summer due to early SOS (Lian et al., 2020) is responsible for the restricted vegetation productivity. Given the strong interaction between phenology, temperature, and SM through atmosphere-vegetation-soil interactions (Seneviratne et al., 2010; Dang et al., 2023), their impact on ecosystem vegetation productivity cannot be analyzed in an isolated manner. Instead, a joint investigation that considers these factors simultaneously is much needed.

In this study, we investigated trends in vegetation productivity (solar-induced chlorophyll fluorescence (SIF), GPP, and net primary productivity (NPP)) in terrestrial ecosystems and their drivers from 2001 to 2019 in the Northern Hemisphere using remotely sensed data, modeled data, and the FLUXNET dataset. We first analyzed the spatial patterns of temperature, SM, vegetation phenology and vegetation productivity and their effects on each other. Then, we analyzed the relationship and importance of phenology, temperature, and SM with vegetation productivity using remote sensing data and verified the results using FLUXNET observation data. Finally, we quantified the spatial patterns of the dominant drivers of vegetation productivity by SOS, EOS, GSL, land surface temperature (LST), and SM using attribution analysis.

2. Materials and method

2.1. Datasets

2.1.1. Solar-induced chlorophyll fluorescence

SIF is considered a great proxy for vegetation productivity in ecosystems (Guanter et al., 2014; Sun et al., 2017; Chen et al., 2021). The global product of SIF (GOSIF) dataset from 2001 to 2019 used in this study was developed using MODIS products and reanalysis data and orbiting carbon ervatory-2(OCO-2) (https://data.globalecology.unh.edu/data/GOSIF_v2/). The GOSIF (hereinafter referred to as SIF) dataset contains three sub-datasets with temporal resolution of 8-day, monthly and yearly, and a spatial resolution of 0.05° (Li and Xiao, 2019). This study used SIF annual temporal resolution data as a proxy for vegetation productivity.

2.1.2. Gross primary productivity and net primary productivity

GPP and NPP represent vegetation productivity, with larger numbers indicating greater productivity. In this study, GPP (2001 to 2019) were obtained from MODIS products (MOD17A2H Version 6, 8-day, 500 m, https://search.earthdata.nasa.gov/). The 8-day cumulative composite values were averaged as annual means with spatial resolution resampled to 0.05° for analysis. In addition, the NPP from 2001 to 2019 were obtained from MODIS products (MOD17A3HGF Version 6, annual, 500 m, https://search.earthdata.nasa.gov/) with a spatial resolution resampling of 0.05° for analysis.

2.1.3. Phenology indicators

The phenology indicators with a spatial resolution of 500 m (2001 to 2019), including SOS, EOS, and GSL, were derived from the MODIS Land Cover Dynamics (MCD12Q2) product (https://search.earthdata.nasa.gov/) (Ganguly et al., 2010). They were resampled at a spatial resolution of 0.05° for analysis.

2.1.4. Land surface temperature

LST were derived from the MODIS Land Surface Temperature (MOD11C3) product (https://search.earthdata.nasa.gov/) from 2001 to 2019, which has a spatial resolution of 0.05°. The correlation coefficient between LST and air temperature (Ts) from FLUXNET dataset is 0.946 ($P < 0.01$, Fig. S1). It should be noted that LST denotes vegetation canopy temperature and Ts denotes air temperature. Moreover, the LST from the MODIS was reported to correlate closely with the Ts (Sims et al., 2008; Ueyama et al., 2010). Therefore, LST is a good substitute for Ts for the analysis.

2.1.5. Soil moisture

SM from 2001 to 2019 were obtained from the TerraClimate with a spatial resolution of 0.05° (Abatzoglou et al., 2018). The TerraClimate dataset shows a significant improvement in the overall mean absolute error and increased spatial realism relative to the coarser resolution gridded dataset (Abatzoglou et al., 2018).

2.1.6. Vegetation type

The vegetation cover types were derived from the MODIS Land Cover Type (MCD12C1) product with the International Geosphere-Biosphere Programme (IGBP) classification scheme (https://search.earthdata.nasa.gov/). MODIS IGBP land cover data is an annual synthetic product with a spatial resolution of 0.05°. The vegetation types include evergreen needleleaf forests (ENF), evergreen broadleaf forests (EBF), deciduous needleleaf forests (DNF), deciduous broadleaf forests (DBF), mixed forests (MF), closed shrublands (CSH), open shrublands (OSH), woody savannas (WSA), savannas (SAV), grasslands (GRA), wetlands (WET), croplands (CRO), urban and built lands (UBL), and cropland/natural vegetation mosaics (CNV).

2.1.7. Land model

To further identify the controlling factors for the temporal dynamics of vegetation productivity, we used GPP simulated by the land model (CABLE, 2001–2016) under different forcing scenarios (https://zenodo.org/record/3629955#.YykVl8hlL15) (Sitch et al., 2015). The CABLE model was run in four scenarios (S0: constant CO_2, climate change, and land cover change; S1: changing CO_2 concentration only; S2: changing CO_2 concentration and climate factors; S3: changing CO_2 concentration, climate factors, and land cover). These four scenario simulations enable us to quantify the impact of CO_2 fertilization (S1-S0), climate change (S2-S1) and land use cover change (S3-S2).

2.1.8. FLUXNET2015 dataset

Flux tower observations were obtained from the FLUXNET2015 Dataset provided by the Global Energy Observations (https://fluxnet.org/data/fluxnet2015-dataset/). The FLUXNET dataset provides GPP estimates based on the respiration extrapolation method (Reichstein et al., 2005) and the light use efficiency method (Lasslop et al., 2010), and thus the mean values of GPP from these two methods were used as the phenological parameters. In addition, FLUXNET dataset also provides Ts and soil water content data (SWC). It should be noted that both SWC of FLUXNET and the SM of TerraClimate are indicators of soil moisture content, only differing in the names of the different products. To reflect long-term GPP and phenology dynamics, FLUXNET sites (Fig. S2; Table S1) with no less than ten years of data were selected. We used Savitzky-Golay (SG) filtering to smooth the daily GPP curves for all 32 FLUXNET sites and then extracted the waiting parameters using the dynamic threshold method (Cong et al., 2012).

2.2. Data analysis

2.2.1. Optimal fingerprint method

We performed an attribution analysis (IPCC, 2021) to explore the drivers of vegetation productivity (SOS, EOS, GSL, LST, and SM) in the Northern Hemisphere using the OFP method (Allen and Tett, 1999; Zhu et al., 2016). The OFP expresses the observation (Y) as a linear combination of scaled (β_i) responses to external driving factors (x_i), and internal variability (ε):$Y = \sum_{i=1}^{N}\beta_i x_i + \varepsilon$. The scaling factors ($\beta_i$) are estimated on the basis of the total least square method to adjust the amplitude of the responses of vegetation productivity to each driving factor. Where Y and $\times$ are the normalized observed vegetation productivity and drivers, respectively; β represents the response coefficient of the external driver; i indicates the i-th factor ($i = 1,2, \cdots,N$). The coefficient β with a value significantly greater than 0 denotes the strong effect of external drivers on the productivity of the observed vegetation.

2.2.2. Redundancy analysis

We quantitatively assessed the effect of drivers on vegetation productivity via Redundancy analysis (RDA) (Rao, 1964) with the forward selection and determined the contribution of each variable with the corresponding significance using the Monte Carlo substitution test. RDA is principal component analysis of the fitted value matrix of the multivariate multiple linear regression between the response variable matrix and the explanatory variables matrix, and is an extension of multi-response variable (multi-response) regression analysis. The simple and conditioned effects of drivers on vegetation productivity obtained in the RDA allow us to determine the dominant factors with a strong impact on vegetation productivity. The correlation between the explanatory variable (i.e., the drivers) and the response variable (i.e., vegetation productivity) could be approximated by projecting the response variable vertically onto the line covering the arrows of the explanatory variable. Smilauer and Leps (2014) realized the combination of sorting graph technology and multivariate statistical methods. The farther the projection point falls in the direction indicated by the arrow of the explanatory variable, the stronger the correlation; the direction of the arrow represents a positive/negative correlation, with the same direction representing a positive correlation, anisotropic a negative correlation, and at the origin of the coordinates representing no correlation (Ter Braak and Smilauer, 2002).

3. Results and discussion

3.1. Trends of LST, SM, phenology, and productivity based on remote sensing data

The analysis of different remotely sensed and hydrological data points to the spatial patterns of increased LST, decreased SM, lengthened phenology, and increased vegetation productivity at mid to high latitudes (latitude ≥ 25°N) in the Northern Hemisphere (Fig. 1 and Fig. S3). The LST increased by 0.041 K/a ($P < 0.01$) (Fig. S3a) from 2001 to 2019, where MODIS MOD11C3 showed 77.52% (Fig. 1a, i) of the pixels

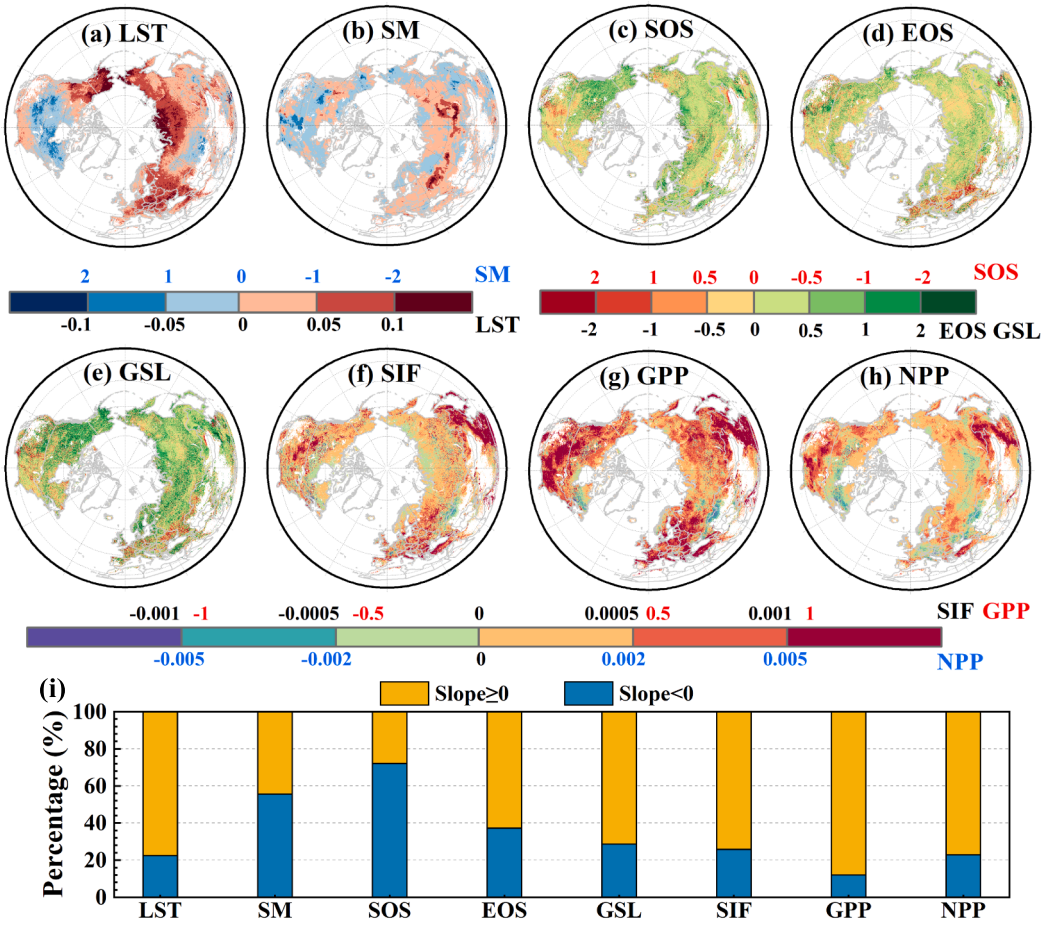

Fig. 1. LST, SM, phenology, and productivity trend patterns in the Northern Hemisphere (latitude ≥ 25°) from 2001 to 2019 based on remote sensing observations. (a) LST of MODIS MOD11C3; (b) SM of Terra Climate; (c) SOS of MODIS MCD12Q2; (d) EOS of MODIS MCD12Q2; (e) GSL (i.e. GSL = EOS- SOS) of MODIS MCD12Q2; (f) SIF; (g) GPP of MODIS MOD17A2H; (h) NPP of MODIS MOD17A3HGF; (i) the ratio of area with positive and negative trends for each indicator. The color of the indicator corresponds to the color of the ribbon bar value.

showing LST increase. However, SM decreased on average by −0.097 mm/a (Fig. S3b), where TerraClimate suggested a decrease in partial SM (55.61% of pixels with reduced SM (Fig. 1b, i).

The SOS was advanced by 0.318 days/a on average ($P < 0.01$; Fig. S3c) from 2001 to 2019, with 72.11% of the pixels showing a trend of advanced SOS (Fig. 1c, i). However, EOS was delayed by 0.133 days/a on average ($P = 0.07$; Fig. S3d), with 62.78% of the pixels showing a delayed trend (Fig. 1d, i). Thus, vegetation GSL was extended on average by 0.499 days/a (Fig. S3e), with 72.41% of the pixels showing extended GSL (Fig, 1e, i). Moreover, SOS ($R = -0.64$, $P < 0.05$), EOS ($R = 0.29$), and GSL ($R = 0.59$, $P < 0.05$) presented correlation with LST (Fig. 2b), indicating that vegetation phenology changes were influenced by increased temperature (Walther et al., 2002; Keenan et al., 2014; Fu et al., 2015). The linear properties of the temperature-phenology relationship suggest that phenology has great potential in the future warming response, although the existence of photoperiodic, cold-heat accumulation, and dormancy constraints may limit this response (Cleland et al., 2007).

The investigated vegetation productivity indicators (SIF, GPP, and NPP) all pointed to an increasing trend of productivity for most of the pixels from 2001 to 2019 (Fig. S3f, g, h). SIF, GPP, and NPP showed increasing trends in 74.15% (Fig. 1f, i), 88.08% (Fig. 1g, i), and 77.09% (Fig. 1h, i) of the pixels, respectively, with a consistent spatial distribution pattern. The observed changes in LST, SM, phenology, and vegetation productivity presented high consistency with those recorded in ground-based flux tower observations (see below), thus enhancing the credibility of the above results from remotely sensed datasets.

From Fig. 2, it was clear that the interaction relationship among LST, SM, SOS, EOS, and GSL with each other and the positive and negative effects on vegetation productivity. The study area showed a trend of LST raising over a large area (Fig. 1a), consistent with the IPCC (2013) report. LST elevation advanced SOS (Fig. 1c) and delayed EOS (Fig. 1d), which in turn lengthened GSL (Fig. 1e). This result was consistent with previous findings that temperature changes altered SOS and EOS (Menzel et al., 2006; Körner and Basler, 2010). The extension of the vegetation growth season would increase vegetation transpiration (vegetation transpiration accounts for approximately 65% of evapotranspiration (Good et al., 2015)) (Fig. S4), leading to a decrease in SM, consistent with previous findings that earlier SOS led to a decrease in SM in summer (Lian et al., 2020). In addition, temperature-evapotranspiration-SM were coupled, with temperature rising to cause an increase in evapotranspiration, which in turn led to a decrease in SM. In turn, a decrease in SM led to a decrease in evapotranspiration, resulting in an elevated temperature (Seneviratne et al., 2010). Changes of vegetation phenology, LST, and SM would affect ecosystem vegetation productivity (Zhang et al., 2022b; Huang et al., 2019; Dang et al., 2022; Gu et al., 2022; Gonsamo et al., 2017). Fig. 2a clearly showed the interaction among them and the impact on productivity. Moreover, Fig. 2b quantified the correlation coefficients between factors with each other further demonstrating the positive and negative effects among them. Thus, temperature-vegetation-SM are coupled to each other, and their spatial patterns and importance for the dominant drivers of vegetation productivity changes remain unclear.

3.2. Trends of Ts, SWC, phenology, and productivity based on FLUXNET data

Trends of daily Ts, SWC, and GPP were analyzed at sites (Fig. S2 and Table S1) with at least ten years of data from the FLUNEXT dataset from 2001 to 2014 (Fig. 3). Ts ($P = 0.8$, Fig. 3a) and SM ($P = 0.2$, Fig. 3b) showed an insignificant increasing trend, while GPP showed a significant increasing trend ($P < 0.01$, Fig. 3f). Most flux tower sites (Fig. S2) presented increased Ts and while others presented decreased Ts (Fig. 1a). Moreover, SWC failed to show a significant increase (Fig. S2). In addition, trends of SOS, EOS, and GSL were analyzed using the dynamic threshold method (Cong et al., 2012; White et al., 1997). Results suggested that SOS was advanced by 0.543 days/a ($P = 0.13$; Fig. 3c), EOS was delayed by 0.761 days/a ($P < 0.01$; Fig. 3d), and GSL was extended by 1.304 days/a ($P = 0.01$; Fig. 3e). The long-term ground flux tower observations verified the results of satellite remote sensing observations.

3.3. Importance of factors that influence vegetation productivity

We quantified the effects of phenology, LST, and SM on vegetation productivity using remotely sensed observations. From Fig. 4, the correlations between SIF and phenology, LST, and SM were significant ($P < 0.01$), with the strongest positive correlation coefficient between SIF and GSL ($R = 0.539$, $P < 0.01$; Fig. 4c). Moreover, we assessed the responding ability of SIF to SOS, EOS, GSL, LST, and SM using the optimal fingerprint (OFP) method. The response coefficients of SOS ($\beta = 0.123$, $P < 0.01$), GSL ($\beta = 0.444$, $P < 0.01$), LST ($\beta = 0.190$, $P < 0.01$) and SM ($\beta = 0.295$, $P < 0.01$) were significantly greater than 0 (Fig. 4f and Table S2), meaning they were suitable for attribution analysis. The GSL scale coefficient was the maximum, indicating the largest contribution to SIF, followed by SM and LST (Fig. 4f). The EOS scale coefficient ($a = -0.103$) was<0 (Fig. 3f and Table S2), indicating that the effect on SIF changes remained confounded with internal variability and could not be clearly detected. We also quantified the effects of SOS, EOS, GSL, LST, and SM on NPP and attribution analysis, and the results showed consistency with SIF (Fig. S5 and Table S2), with the highest correlation coefficient between NPP and GSL ($R = 0.612$, $P < 0.01$; Fig. S5c) and the

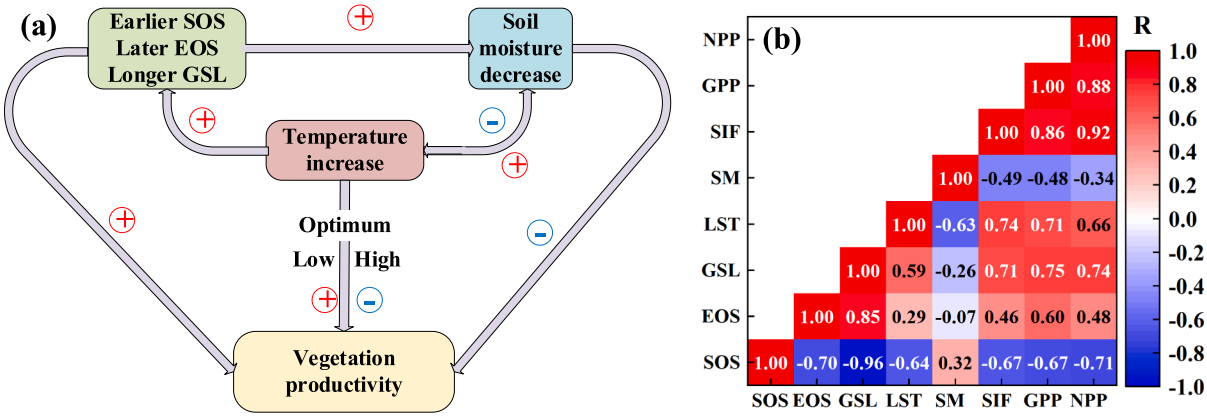

Fig. 2. Interrelationships among LST, vegetation phenology (SOS, EOS, and GSL), SM and effects on vegetation productivity. (a) Positive and negative impact relationships among LST, SM, SOS, EOS, GSL and vegetation productivity. The prefix " +" indicates a positive effect, while "-" indicates otherwise. (b) Correlation coefficients of factors with each other. The absolute value of R greater than 0.456 indicates $P < 0.05$.

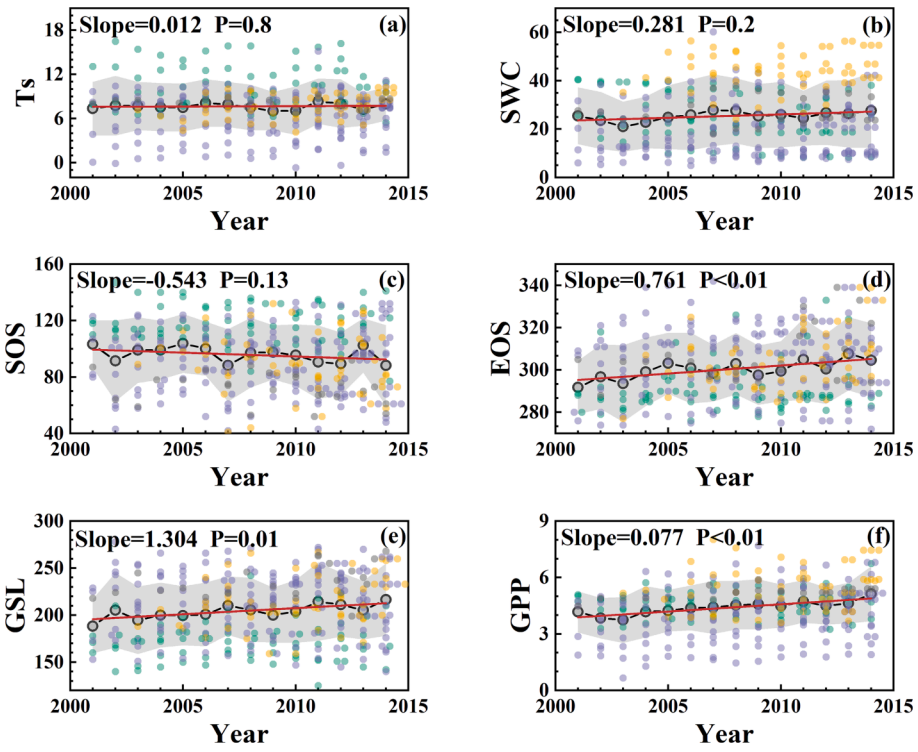

Fig. 3. Long-term trends of meteorology-hydrology, phenology and productivity observed by flux towers. (a) Ts trends; (b) SWC trends; (c) SOS trends; (d) EOS trends; (e) GSL trends; (f) GPP trends. Gray shaded bands indicate doubled standard deviation. The colors of the dots correspond to the colors of the vegetation types (DBF, ENF, GRA, and MF) in the legend.

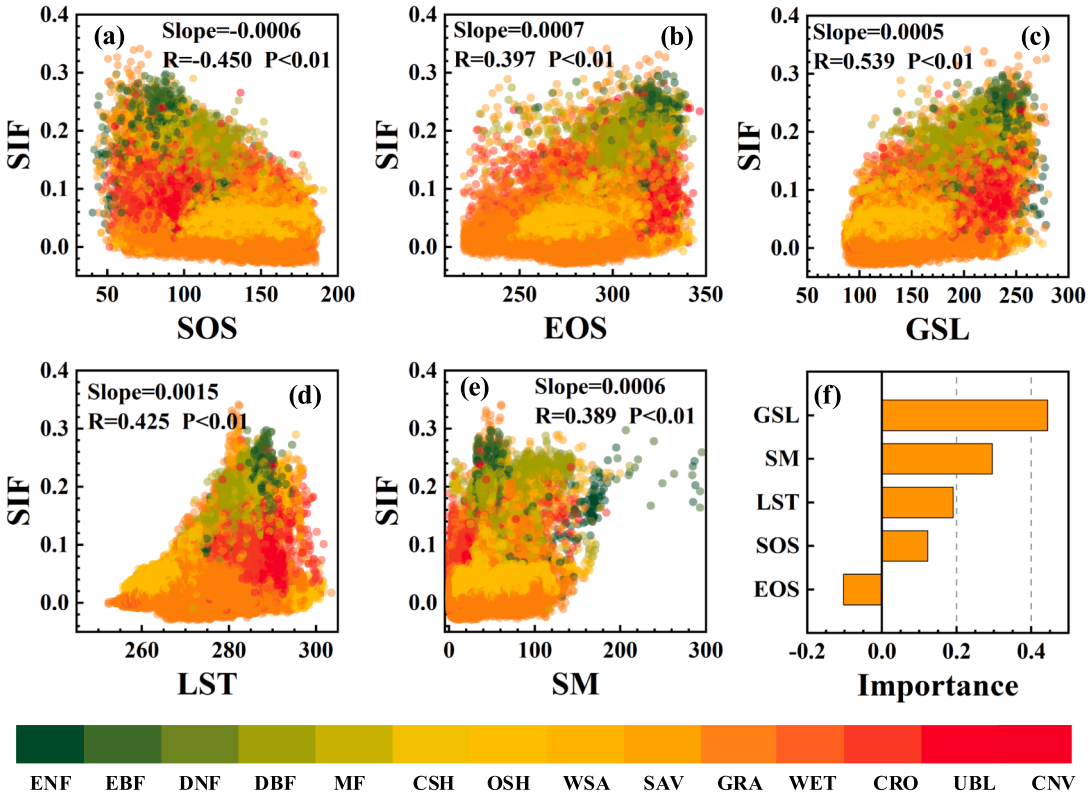

Fig. 4. The relationships among phenology, LST, SM and vegetation productivity from remote sensing data. (a) correlation coefficient between SOS and SIF; (b) correlation coefficient between EOS and SIF; (c) correlation coefficient between GSL and SIF; (d) correlation coefficient between LST and SIF; (e) correlation coefficient between SM and SIF; (f) importance of SOS, EOS, GSL, LST, and SM on SIF assessed using the OFP method. LST, SM, and SIF are the annual means. The vegetation types include ENF, EBF, DNF, DBF, MF, CSH, OSH, WSA, SAV, GRA, WET, CRO, UBL, and CNV.

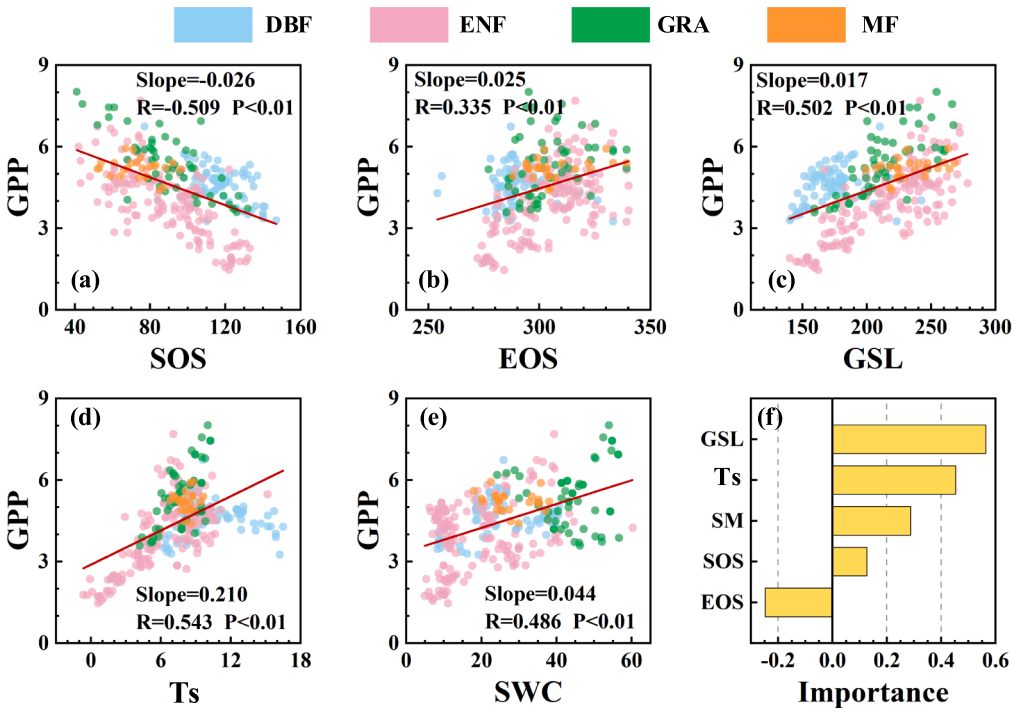

Fig. 5. The relationships among phenology, Ts, SM, and vegetation productivity from flux towers data. (a) correlation coefficient between SOS and GPP; (b) correlation coefficient between EOS and GPP; (c) correlation coefficient between GSL and GPP; (d) correlation coefficient between Ts and GPP; (e) correlation coefficient between SWC and GPP; (f) importance of SOS, EOS, GSL, Ts, and SWC on GPP assessed using OFP method. Ts, SWC, and GPP are the annual means. The vegetation types include ENF, DBF, MF, and GRA.

maximum scale coefficient of OFP attribution analysis ($\beta = 0.489$, $P < 0.01$; (Table S2). In summary, the analysis showed that earlier SOS, delayed EOS, and longer GSL could increase vegetation productivity, which was consistent with the study by Keenan et al. (2014). GSL was identified as the most important driver of vegetation productivity changes, followed by SM and LST.

In addition, we used RDA to rank the significance of the effects of SOS, EOS, GSL, LST, and SM on vegetation productivity (SIF and NPP) (Table S4 and Fig. S6). The results showed that SIF and NPP responded consistently to each factor with a total explanation of 39.17% and 43.17%, respectively. GSL, SOS, LST and SM were significant at the 0.01 level, indicating their strongest effect on vegetation productivity (SIF and NPP) variation, with GSL having an explainable degree of up to 29.1% and 37.67%, respectively, followed by SM (6.73% and 4.73%) and LST (2.73% and 0.97%). SOS and EOS explained no more than 0.5%. Thus, we could conclude that GSL was the most important factor contributing to vegetation productivity changes, followed by SM and LST. The results from the OFP method and RDA were highly consistent.

We also quantified the effects of phenology, Ts, and SWC on vegetation productivity from long-term FLUXNET data. As shown in Fig. 5, the correlation between GPP and SOS was negative ($R = -0.509$, $P < 0.01$). However, the correlation between GPP and EOS ($R = 0.335$, $P < 0.01$), GSL ($R = 0.502$, $P < 0.01$), Ts ($R = 0.543$, $P < 0.01$), SWC ($R = 0.486$, $P < 0.01$) were positive. Thus, advanced SOS and extended EOS and GSL corresponded to increased vegetation productivity. In addition, increased Ts and SWC are also responsible for enhanced vegetation productivity. The attribution analysis using OFP showed that GSL ($\beta = 0.564$, $P < 0.01$) extension was the most important factor for the increase in vegetation GPP (Fig. 5f and Table S3), followed by Ts ($\beta = 0.453$, $P < 0.01$) and SWC ($\beta = 0.288$, $P < 0.01$). However, the EOS scale coefficient ($\beta = -0.247$) was<0 (Fig. 5f and Table S3), indicating that the effect on GPP changes remained confounded with internal variability and could not be clearly detected. The analytical results based on flux tower data indicated that GSL was the most important driver of vegetation productivity changes, followed by SWC and Ts.

We further used RDA to rank the importance of the effects of SOS, EOS, GSL, Ts, and SWC on vegetation productivity (GPP) (Table S4 and Fig. S7). SWC explained the most of GPP (26%, $P < 0.01$), followed by Ts (18.5%, $P < 0.01$) and SOS (9.9%, $P < 0.01$). The RDA based on flux tower data revealed that SWC and Ts were the drivers of main vegetation productivity. The above findings from flux tower sites differ from the ones from remotely sensed observations. It might be mainly caused by the location of ground stations. For example, Piao et al. (2018) revealed that delayed EOS is responsible for the increase in vegetation carbon emissions, while Zhang et al. (2020) observed that it was mainly caused by the location of ground stations.

3.4. Spatial patterns of the dominant drivers of vegetation productivity

It is crucial to identify the dominant factors that cause changes in vegetation productivity. We used the OFP method to further study the dominant drivers of vegetation productivity changes at the pixel scale for SOS, EOS, GSL, LST, and SM. Our results showed that the percentage of positively influenced pixels (56.97% (SIF) and 58.70% (NPP)) of these factors on the dominant drivers of vegetation productivity at mid to high latitudes in the Northern Hemisphere were greater than the negative effects (43.03% (SIF) and 41.30% (NPP)) (Fig. 6). Meanwhile, the percentage of positive effects pixels of SOS, EOS, GSL, and LST on vegetation productivity were all greater than the negative effects (Fig. S8 and Fig. S9), except for SM, whose percentage of positive effects pixels on vegetation productivity (45.3% (SIF) and 42.2% (NPP)) were slightly weaker than the negative effects (54.7% (SIF) and 57.8% (NPP)) (Fig. S8 and Fig. S9). 55% of pixels exhibited reduced SM, and reduced SM can limit vegetation productivity (Liu et al., 2020a; Reich et al., 2018). The above findings were consistent with the area and spatial distribution where SM played a negative role (Fig. 1b, Fig. S8f, and Fig. S9f). Thus, the interaction of several factors pointed to an overall increasing trend of vegetation productivity (Fig. 1).

The analysis at middle and high latitudes showed that phenological change is a dominant driver of increased vegetation productivity, showing a spatially homogeneous effect (Fig. 6, Fig. S8, and Fig. S9). From 2001 to 2019, phenology changes dominated 65.78% (SIF) and 62.02% (NPP) of pixels of the changes in vegetation productivity at mid to high latitudes in the Northern Hemisphere, respectively, where the percentage of positive effects pixels on vegetation productivity as the dominant driver reached 41.20% (SIF) and 40.42% (NPP), respectively.

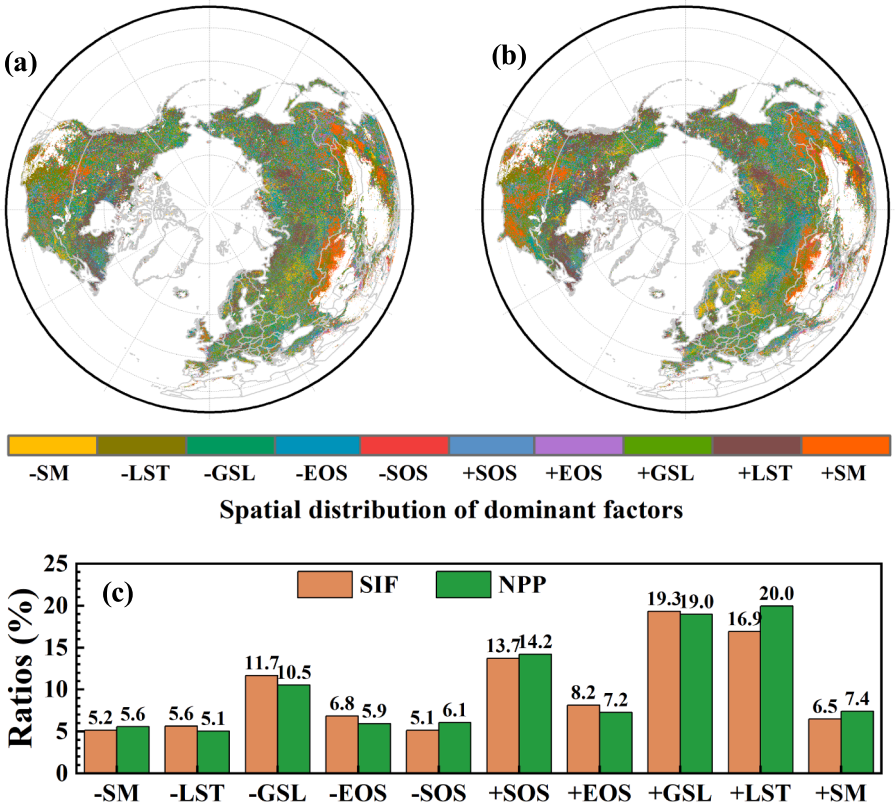

Fig. 6. Spatial pattern of the dominant drivers of vegetation productivity changes. (a) The main driver of SIF, defined as the driver that contributes most to the change of SIF in each vegetation pixel; (b) the main driver of NPP, defined as the driver that contributes most to the change of NPP in each vegetation pixel; (c) the ratio of the area of vegetation photosynthesis change that is mainly driven by each factor. The drivers include phenology (SOS, EOS, and GSL), LST, SM. Vegetation photosynthesis is represented by SIF and NPP. The prefix "+" indicates a positive effect on vegetation photosynthesis, while "-" indicates otherwise.

Moreover, the proportions of positive effects pixels (51.4%-62.4%) of SOS, EOS, and GSL on vegetation productivity were greater than proportions of negative effects pixels (37.6%-48.6%) (Fig. S8 and Fig. S9), consistent with the results of existing studies (Keenan et al., 2014; Gonsamo et al., 2017). GSL was found to be the most important factor for changes in vegetation productivity (Fig. 6), consistent with the results above (Fig. 4f and Fig. 5f).

LST was the dominant driver of vegetation productivity accounting for 22.56% (SIF) and 25.02% (NPP) of the vegetated areas, with a mainly proportions of positive effect pixels (75.06% (SIF) and 79.79% (NPP)) (Fig. 6). The positive effects of LST were mainly distributed in the high-latitude regions, while the negative effects were mainly distributed in the low-latitude regions (Fig. S8d and Fig. S9d). The proportions of positive effect pixels of LST (68.4% (SIF) and 69.7% (NPP)) on vegetation productivity at middle and high latitudes in the Northern Hemisphere was the largest area of each indicator (Fig. S8 and Fig. S9). However, GSL was the dominant driver of vegetation productivity for the largest area (Fig. 6). As rising temperatures at high latitudes could extend the length of the vegetation growing season and enhance productivity (Xu et al., 2013) and higher latitude ecosystem temperatures below the optimum temperature (Huang et al., 2019), positive temperature effects were mainly distributed in high latitude regions.

Dang et al. (2022) revealed that temperatures played a greater role in vegetation productivity than SM at mid to high latitudes in the northern hemisphere. Our results showed that SM was the dominant driver of vegetation productivity for only 11.66% (SIF) and 12.96% (NPP) of the vegetated area, smaller than the area where the temperature was the dominant driver (Fig. 6). Moreover, the percentage of area positively affected by SM on SIF and NPP was 45.3% and 42.2%, respectively, smaller than the negative effect (54.7% and 57.8%) (Fig. S8 and Fig. S9), which was consistent with the area of SM reduction trend (55.61%) (Fig. 1b and i). Studies have shown that reduced SM decreases productivity in vegetation (Liu et al., 2020a; Reich et al., 2018; Ngolo and Watanabe, 2022), explaining our observations that negative effects are dominant for SM on SIF and NPP.

Keenan and Riley (2018) revealed a positive effect of growing season temperature on productivity in high-latitude ecosystems. The results from this study demonstrated that temperature did have a positive effect on vegetation productivity in high-latitude vegetation in the Northern Hemisphere (Fig. 6, Fig. S8, and Fig. S9). However, the attribution analysis showed that vegetation phenology changes were the dominant factor associated with changes in ecosystem productivity, possibly related to the reduced temperature dependence of productivity in Northern Hemisphere ecosystems (Piao et al., 2017).

In addition, CO_2 concentration (Keenan et al., 2021; Zhang et al., 2022a), climate change (Xu et al., 2019) land use cover change (Yue et al., 2020) all affected vegetation productivity. We then used the CABLE model to capture the spatial pattern of increased GPP (Fig. 7). We employed different scenarios of CABLE model and means (i.e., multi-scenarios ensemble GPP of means, MSEM) to determine factors for the trend of increasing GPP. The trend of GPP derived from MSEM (Slope = 0.00036, $R = 0.951$, $P < 0.01$) was consistent with the trend obtained from satellite products and flux towers (Fig. 1, Fig. 3, and Fig. 7). Moreover, 84.26% of pixels of the MSEM-derived GPP showed an increasing trend (Fig. 7c), which was generally consistent with those of the remote sensing products vegetation productivity (SIF, GPP, and NPP), with a consistent spatial pattern of increase (Fig. 1f, g, h). The CABLE model successfully revealed that different scenarios captured the mechanisms of increased vegetation productivity over the last 20 years.

The model experiments by changing forcing scenarios demonstrated that CO_2 fertilization was the main contributor to the increase in GPP, while climate change and land use cover change had little contribution (Fig. 7b). In conclusion, compared to the S0 scenario GPP values, CO_2 fertilization increased GPP by 32.33%, followed by climate change (5.29%) and land use cover change (2.41%). Also, spatially relative to the S0 scenario GPP values, CO_2 fertilization played a positive role in vegetation productivity for 99.82% of pixels (Fig. 7d), followed by climate change (87.13%) and land use cover change (56.01%) (Fig. 7e,

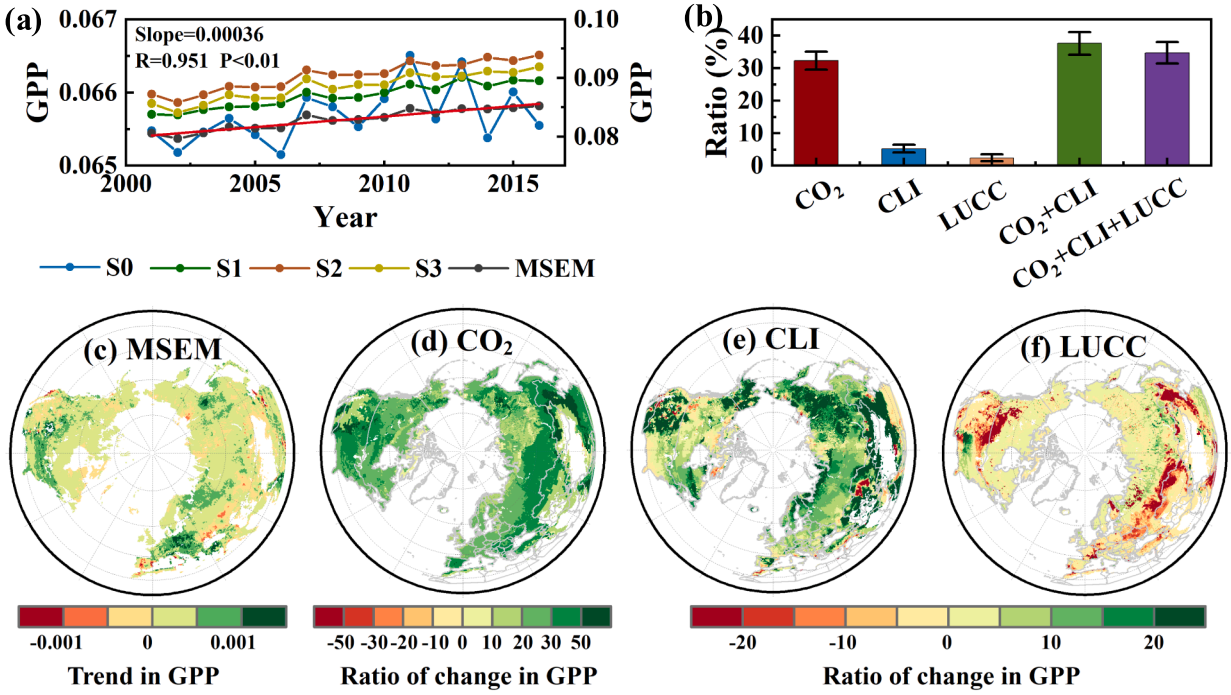

Fig. 7. Spatial patterns of GPP and contributing factors estimated with land model. The black and red line in (a) indicates the dynamic of the multi-scenarios ensemble mean (MSEM) and linear fit line, respectively. (b) Simulated contributions to GPP driven by rising CO_2, climate change (CLI), and land use cover change (LUCC) individually and in combination. (c) Spatial pattern of GPP trend estimated with MSEM. (d) Spatial pattern of GPP changes as impacted by CO_2. (e) Spatial pattern of GPP changes as impacted by CLI. (f) Spatial pattern of GPP changes as impacted by LUCC. (For interpretation of the references to color in this figure legend, the reader is referred to the web version of this article.)

f).

In addition, atmospheric nitrogen deposition can increase the sensitivity of vegetation productivity to climate change by reducing the stability of dominant species (Liu et al., 2019), which in turn affects vegetation productivity. Moreover, with continued warming, radiative limitation will increase, leading to a widespread radiative limitation in ecosystem productivity that can affect vegetation productivity (Zhang et al., 2020). And other factors not considered at the regional scale affect vegetation productivity, such as disturbances in tillage practices, irrigation, pests and diseases, forest management, fire, urbanization (Zhuang et al., 2022a; Shao et al., 2021), and salinization (Zhuang et al., 2022b), might be the reason for the mismatch between observed and attributed analyses of vegetation productivity changes.

Finally, we should also consider the sensitivity, uncertainty and causality of drivers on vegetation productivity, while considering the nonlinear and spatial–temporal variation relationships between vegetation productivity and drivers. First of all, we should carry out sensitivity and uncertainty analysis of multiple drivers to identify the key determinants affecting vegetation productivity changes to address the model/analysis uncertainty-sensitivity-correlation coupling problem (Pianosi et al., 2016). The variance method is available to investigate the variability generated by the variability of drivers on vegetation productivity to identify the major vegetation productivity drivers. Then, non-linearity between determinants and vegetation productivity is considered (Koch et al., 2009; Newbold et al., 2020). At present, convergent cross mapping, optimal information flow (OIF) (Li and Convertino, 2021), PCMCI (Runge et al., 2019), empirical dynamical modeling, and other machine learning models are able to account for the nonlinearities between vegetation productivity and driver interactions. Moreover, they may also have time lag problems (Guo et al., 2020). Therefore, it is important to predict ecosystem vegetation productivity with nonlinear models that consider time lags, based on the integration of determinants identified by sensitivity analysis. Finally, both vegetation productivity and drivers vary in spatial and temporal terms (Zeng et al., 2022). Therefore, vegetation productivity can be analyzed as a function of the variables of the drivers, considering the joint probability distribution function or mean and variance, and the study refers to the variability of the drivers as a function of the vegetation productivity gradient. It is important to quantify the stability of ecological patterns of vegetation productivity gradients. This is because this enables the definition of potential steady states, where vegetation productivity does not change, critical points, and other potential unobserved states that need to be utilized to determine vegetation productivity. Therefore, we will further study these deficiencies in our future work.

4. Conclusions

Under the context of global climate change, it is essential to understand the mechanisms of vegetation productivity changes so that a better understanding of the impact of climate change on productivity in terrestrial ecosystems can be achieved. In this study, we quantitatively assessed the importance of phenology and environmental factors on vegetation productivity. Cross-validated results obtained from remotely sensed observations and flux towers data indicated that phenology was the dominant driver, despite the differences in the importance of temperature and SM between remotely sensed and flux tower observations. Vegetation productivity models considering vegetation phenology might further improve the assessment accuracy.

CRediT authorship contribution statement

Chaoya Dang: Conceptualization, Methodology, Writing – review & editing, Writing – original draft. **Zhenfeng Shao:** Conceptualization, Funding acquisition, Supervision, Project administration, Resources. **Xiao Huang:** Validation. **Qingwei Zhuang:** Validation, Data curation. **Gui Cheng:** Validation, Data curation. **Jiaxin Qian:** Validation, Data curation.

Declaration of Competing Interest

The authors declare that they have no known competing financial interests or personal relationships that could have appeared to influence the work reported in this paper.

Data availability

GOSIF data are available at http://data.globalecology.unh.edu/data/GOSIF_v2/; MODIS data are available at https://search.earthdata.nasa.gov/; FLUXNET2015 Dataset are available at https://fluxnet.org/data/fluxnet2015-dataset/; TerraClimate data are available at https://climatedataguide.ucar.edu/.

Acknowledgements

This work was supported in part by the National Natural Science Foundation of China under Grants 42090012; in part by the Guangxi science and technology program under Grants 2021AB30019; 03 special research and 5G project of Jiangxi Province in China under Grants 20212ABC03A09; Zhuhai industry university research cooperation project of China under Grants ZH22017001210098PWC; Sichuan Science and Technology Program under Grants 2022YFN0031, 2023YFS0381, and 2023YFN0022; Hubei key R & D plan under Grants 2022BAA048; Shanxi Province Science and Technology Major Special Project under Grants 202201150401020, and Guangxi Key Laboratory of Spatial Information and Mapping Fund Project under Grants 21-238-21-01.

Appendix A. Supplementary data

Supplementary data to this article can be found online at https://doi.org/10.1016/j.ecolind.2023.110326.

References

Abatzoglou, J.T., Dobrowski, S.Z., Parks, S.A., Hegewisch, K.C., 2018. TerraClimate, a high-resolution global dataset of monthly climate and climatic water balance from 1958–2015. Sci. Data 5, 170191.

Albergel, C., Dorigo, W., Reichle, R.H., Balsamo, G., de Rosnay, P., Muñoz-Sabater, J., Isaksen, L., de Jeu, R., Wagner, W., 2013. Skill and global trend analysis of soil moisture from reanalyses and microwave remote sensing. J. Hydrometeorol. 14 (4), 1259–1277.

Allen, M.R., Tett, S.F.B., 1999. Checking for model consistency in optimal fingerprinting. Clim. Dyn. 15 (6), 419–434.

Barichivich, J., Briffa, K.R., Myneni, R.B., Osborn, T.J., Melvin, T.M., Ciais, P., Piao, S., Tucker, C., 2013. Large-scale variations in the vegetation growing season and annual cycle of atmospheric CO_2 at high northern latitudes from 1950 to 2011. Glob. Chang Biol. 19 (10), 3167–3183.

Braswell, B.H., Schimel, D.S., Linder, E., Moore Iii, B., 1997. The response of global terrestrial ecosystems to interannual temperature variability. Science 278 (5339), 870–873.

Came, R.E., Eiler, J.M., Veizer, J., Azmy, K., Brand, U., Weidman, C.R., 2007. Coupling of surface temperatures and atmospheric CO_2 concentrations during the Palaeozoic era. Nature 449 (7159), 198–201.

Chen, A., Mao, J., Ricciuto, D., Xiao, J., Frankenberg, C., Li, X., Thornton, P.E., Gu, L., Knapp, A.K., 2021. Moisture availability mediates the relationship between terrestrial gross primary production and solar-induced chlorophyll fluorescence: Insights from global-scale variations. Glob. Chang Biol. 27 (6), 1144–1156.

Cleland, E.E., Chuine, I., Menzel, A., Mooney, H.A., Schwartz, M.D., 2007. Shifting plant phenology in response to global change. Trends Ecol. Evol. 22 (7), 357–365.

Cong, N., Piao, S., Chen, A., Wang, X., Lin, X., Chen, S., Han, S., Zhou, G., Zhang, X., 2012. Spring vegetation green-up date in China inferred from SPOT NDVI data: A multiple model analysis. Agric. For. Meteorol. 165, 104–113.

Dang, C., Shao, Z., Huang, X., Qian, J., Cheng, G., Ding, Q., Fan, Y., 2022. Assessment of the importance of increasing temperature and decreasing soil moisture on global ecosystem productivity using solar-induced chlorophyll fluorescence. Glob. Chang Biol. 28, 2066–2080.

Dang, C., Shao, Z., Huang, X., Zhuang, Q., Cheng, G., Qian, J., 2023. Vegetation greenness and photosynthetic phenology in response to climatic determinants. Front. For. Glob. Change 6, 75.

dela Torre, D.M.G., Gao, J., Macinnis-Ng, C., 2021. Remote sensing-based estimation of rice yields using various models: A critical review. Geo. Spat. Inf. Sci. 24 (4), 580–603.

Deng, Y., Wang, S., Bai, X., Luo, G., Wu, L., Cao, Y., Li, H., Li, C., Yang, Y., Hu, Z., Tian, S., 2020. Variation trend of global soil moisture and its cause analysis. Ecol. Indic. 110, 105939.

Dragoni, D., Schmid, H.P., Wayson, C.A., Potter, H., Grimmond, C., Randolph, J.C., 2011. Evidence of increased net ecosystem productivity associated with a longer vegetated season in a deciduous forest in south-central indiana, usa. Glob. Chang Biol. 17 (2), 886–897.

Fu, Y.H., Zhao, H., Piao, S., Peaucelle, M., Peng, S., Zhou, G., Ciais, P., Huang, M., Menzel, A., Peñuelas, J., Song, Y., Vitasse, Y., Zeng, Z., Janssens, I.A., 2015. Declining global warming effects on the phenology of spring leaf unfolding. Nature 526 (7571), 104–107.

Ganguly, S., Friedl, M.A., Tan, B., Zhang, X., Verma, M., 2010. Land surface phenology from MODIS: Characterization of the Collection 5 global land cover dynamics product. Remote Sens. Environ. 114 (8), 1805–1816.

Goetz, S.J., Prince, S.D., 1999. Modelling terrestrial carbon exchange and storage: evidence and implications of functional convergence in light-use efficiency. Adv. Ecol. Res. 28, 57–92.

Gonsamo, A., Chen, J.M., Ooi, Y.W., 2017. Peak season plant activity shift towards spring is reflected by increasing carbon uptake by extratropical ecosystems. Glob. Chang Biol. 24 (5), 2117–2128.

Good, S.P., Noone, D., Bowen, G., 2015. Hydrologic connectivity constrains partitioning of global terrestrial water fluxes. Science 349 (6244), 175–177.

Green, J.K., Seneviratne, S.I., Berg, A.M., Findell, K.L., Hagemann, S., Lawrence, D.M., Gentine, P., 2019. Large influence of soil moisture on long-term terrestrial carbon uptake. Nature 565 (7740), 476–479.

Gu, H., Qiao, Y., Xi, Z., Rossi, S., Smith, N.G., Liu, J., Chen, L., 2022. Warming-induced increase in carbon uptake is linked to earlier spring phenology in temperate and boreal forests. Nat. Commun. 13 (1), 3698.

Guanter, L., Zhang, Y., Jung, M., Joiner, J., Voigt, M., Berry, J.A., Frankenberg, C., Huete, A.R., Zarco-Tejada, P., Lee, J.E., Moran, M.S., Ponce-Campos, G., Beer, C., Camps-Valls, G., Buchmann, N., Gianelle, D., Klumpp, K., Cescatti, A., Baker, J.M., Griffis, T.J., 2014. Global and time-resolved monitoring of crop photosynthesis with chlorophyll fluorescence. Proc. Natl. Acad. Sci. U.S.A. 111(14), E1327-E1333.

Guo, L., Gao, J., Ma, S., Chang, Q., Zhang, L., Wang, S., Zou, Y., Wu, S., Xiao, X., 2020. Impact of spring phenology variation on GPP and its lag feedback for winter wheat over the North China Plain. Sci. Total Environ., 138342

He, B., Chen, C., Lin, S., Yuan, W., Chen, H.W., Chen, D., Zhang, Y., Guo, L., Zhao, X., Liu, X., Piao, S., Zhong, Z., Wang, R., Tang, R., 2022. Worldwide impacts of atmospheric vapor pressure deficit on the interannual variability of terrestrial carbon sinks. Natl. Sci. Rev. 9 (4) nwab150.

Huang, M., Piao, S., Ciais, P., Peñuelas, J., Wang, X., Keenan, T.F., Peng, S., Berry, J.A., Wang, K., Mao, J.F., Alkama, R., Cescatti, A., Cuntz, M., Hannes, D.D., Gao, M., He, Y., Liu, Y., Luo, Y., Myneni, R.B., Janssens, I.A., 2019. Air temperature optima of vegetation productivity across global biomes. Nat. Ecol. Evol. 3 (5), 772–779.

Ipcc, 2021. Summary for Policymakers. Climate Change 2021: The Physical Science Basis. Contribution of Working Group I to the Sixth Assessment Report of the Intergovernmental Panel on Climate Change. Cambridge University Press. In Press.

IPCC Climate Change 2013: The Physical Science Basis. Contribution of working Group I to the Fifth Assessment Report of the Intergovernmental Panel on Climate Change (eds Stocker, T.F. et al.) (Cambridge Univ. Press, 2013).

Jia, B., Zhou, G., 2023. Estimation of global karst carbon sink from 1950s to 2050s using response surface methodology. Geo. Spat. Inf. Sci. 1–18.

Keenan, T.F., Luo, X., Kauwe, M.G., Medlyn, B.E., Prentice, I.C., Stocker, B.D., Smith, N., Terrer, C., Wang, H., Zhang, Y., Zhou, S., 2021. A constraint on historic growth in global photosynthesis due to increasing CO_2. Nature 600, 253–258.

Keenan, T.F., Riley, W.J., 2018. Greening of the land surface in the world's cold regions consistent with recent warming. Nat. Clim. Change 8 (9), 825–828.

Keenan, T.F., Gray, J., Friedl, M.A., Toomey, M., Bohrer, G., Hollinger, D.Y., Munger, J. W., O'Keefe, J., Schmid, H.P., Wing, I.S., Yang, B., Richardson, A.D., 2014. Net carbon uptake has increased through warming-induced changes in temperate forest phenology. Nat. Clim. Change 4 (7), 598–604.

Koch, E.W., Barbier, E.B., Silliman, B.R., Reed, D.J., Perillo, G.M., Hacker, S.D., Granek, E.F., Primavera, J.H., Muthiga, N., Polaske, S., Halpern, B.S., Kennedy, C.J., Kappel, C.V., Wolanski, E., 2009. Non-linearity in ecosystem services: temporal and spatial variability in coastal protection. Front. Ecol. Environ. 7 (1), 29–37.

Körner, C., Basler, D., 2010. Phenology under global warming. Science 327 (5972), 1461–1462.

Lasslop, G., Reichstein, M., Papale, D., Richardson, A.D., Arneth, A., Barr, A., Stoy, P., Wohlfahrt, G., 2010. Separation of net ecosystem exchange into assimilation and respiration using a light response curve approach: critical issues and global evaluation. Glob. Chang Biol. 16 (1), 187–208.

Li, J., Convertino, M., 2021. Inferring ecosystem networks as information flows. Sci. Rep. 11 (1), 7094.

Li, X., Xiao, J., 2019. A Global, 0.05-Degree Product of Solar-Induced Chlorophyll Fluorescence Derived from OCO-2, MODIS, and Reanalysis Data. Remote Sens. 11 (5), 517.

Lian, X., Piao, S., Li, L.Z.X., Li, Y., Huntingford, C., Ciais, P., Cescatti, A., Janssens, I.A., Peñuelas, J., Buermann, W., Chen, A., Li, X., Myneni, R.B., Wang, X., Wang, Y., Yang, Y., Zeng, Z., Zhang, Y., McVicar, T.R., 2020. Summer soil drying exacerbated by earlier spring greening of northern vegetation. Sci. Adv. 6 (1), eaax0255.

Liu, L., Gudmundsson, L., Hauser, M., Qin, D., Li, S., Seneviratne, S.I., 2020a. Soil moisture dominates dryness stress on ecosystem production globally. Nat. Commun. 11 (1), 4892.

Liu, Y., Kumar, M., Katul, G.G., Feng, X., Konings, A.G., 2020b. Plant hydraulics accentuates the effect of atmospheric moisture stress on transpiration. Nat. Clim. Change 10 (7), 691–695.

Liu, J., Li, X., Ma, Q., Zhang, X., Chen, Y., Isbell, F., Wang, D., Le Bagousse-Pinguet, Y., 2019. Nitrogen addition reduced ecosystem stability regardless of its impacts on plant diversity. J. Ecol. 107 (5), 2427–2435.
Menzel, A., Sparks, T.H., Estrella, N., Koch, E., Aasa, A., Ahas, R., Alm-K Kübler, K., Bissolli, P., Braslavská, O., Briede, A., Chmielewski, F.M., Crepinsek, Z., Curnel, Y., Dahl, A., Defila, C., Donnelly, A., Filella, Y., Jatczak, K., Mage, F., Mestre, A., Nordli, Ø., Peñuelas, J., Pirinen, P., Remisova, V., Scheifinger, H., Striz, M., Susnik, A., Vliet, A.J.H.V., Wielgolaski, F.-E., Zach, S., Zust, A.N.A., 2006. European phenological response to climate change matches the warming pattern. Glob. Chang Biol. 12 (10), 1969–1976.
Nemani, R.R., Keeling, C.D., Hashimoto, H., Jolly, W.M., Piper, S.C., Tucker, C.J., Myneni, R.B., Running, S.W., 2003. Climate-driven increases in global terrestrial net primary production from 1982 to 1999. Science 300 (5625), 1560–1563.
Newbold, T., Tittensor, D.P., Harfoot, M.B.J., Scharlemann, J.P.W., Purves, D.W., 2020. Non-linear changes in modelled terrestrial ecosystems subjected to perturbations. Sci. Rep. 10 (1), 14051.
Ngolo, A.M.E., Watanabe, T., 2022. Integrating geographical information systems, remote sensing, and machine learning techniques to monitor urban expansion: an application to Luanda. Angola. Geo. Spat. Inf. Sci. 1–19.
Pianosi, F., Beven, K., Freer, J., Hall, J.W., Rougier, J., Stephenson, D.B., Wagener, T., 2016. Sensitivity analysis of environmental models: A systematic review with practical workflow. Environ. Model. Softw. 79, 214–232.
Piao, S., Ciais, P., Friedlingstein, P., Peylin, P., Reichstein, M., Luyssaert, S., Margolis, H., Fang, J., Barr, A., Chen, A., Grelle, A., Hollinger, D.Y., Laurila, T., Lindroth, A., Richardson, A.D., Vesala, T., 2008. Net carbon dioxide losses of northern ecosystems in response to autumn warming. Nature 451 (7174), 49–52.
Piao, S., Liu, Z., Wang, T., Peng, S., Ciais, P., Huang, M., Ahlstrom, A., Burkhart, J.F., Cgevallier, F., Janssens, I.A., Jeong, S.-J., Lin, X., Mao, J., Miller, J., Mohammat, A., Myneni, R.B., Peñuelas, J., Shi, X., Stohl, A., Yao, Y., Zhu, Z., Tans, P.P., 2017. Weakening temperature control on the interannual variations of spring carbon uptake across northern lands. Nat. Clim. Change 7 (5), 359–363.
Rao, C. R., 1964. The use and interpretation of principal component analysis in applied research. Sankhyā: The Indian Journal of Statistics, Series A (1961-2002) 26 (4), 329-358.
Reich, P.B., Sendall, K.M., Stefanski, A., Rich, R.L., Hobbie, S.E., Montgomery, R.A., 2018. Effects of climate warming on photosynthesis in boreal tree species depend on soil moisture. Nature 562 (7726), 263–267.
Reichstein, M., Falge, E., Baldocchi, D., Papale, D., Aubinet, M., Berbigier, P., Bernhofer, C., Buchmann, N., Gilmanov, T., Granier, A., Grünwald, T., Havránková, K., Ilvesniemi, H., Janous, D., Knohl, A., Laurila, T., Lohila, A., Loustau, D., Matteucci, G., Meyers, T., Miglietta, F., Ourcival, J.-M., Pumpanen, J., Rambal, S., RoTenberg, E., Sanz, M., Tenhunen, J., Seufert, G., Vaccar, F., Vesala, T., Yakir, D., Valentini, R., 2005. On the separation of net ecosystem exchange into assimilation and ecosystem respiration: review and improved algorithm. Glob. Change Biol. 11 (9), 1424–1439.
Richardson, A.D., Andy Black, T., Ciais, P., Delbart, N., Friedl, M.A., Gobron, N., Hollinger, D.Y., Kutsch, W.L., Longdoz, B., Luyssaert, S., Migliavacca, M., Montagnani, L., Munger, J.W., Moors, E., Piao, S., Rebmann, C., Reichstein, M., Saigusa, N., Tomelleri, E., Vargas, R., Varlagin, A., 2010. Influence of spring and autumn phenological transitions on forest ecosystem productivity. Philosophical Transactions of the Royal Society B: Biological Sciences 365 (1555), 3227–3246.
Runge, J., Nowack, P., Kretschmer, M., Flaxman, S., Sejdinovic, D., 2019. Detecting and quantifying causal associations in large nonlinear time series datasets. Sci. Adv. 5 (11) eaau4996.
Scalon, M.C., Oliveras Menor, I., Freitag, R., Peixoto, K.S., Rifai, S.W., Marimon, B.S., Marimon Junior, B.H., Malhi, Y., 2022. Contrasting strategies of nutrient demand and use between savanna and forest ecosystems in a neotropical transition zone. Biogeosciences 19 (15), 3649–3661.
Seneviratne, S.I., Corti, T., Davin, E.L., Hirschi, M., Jaeger, E.B., Lehner, I., Orlowsky, B., Teuling, A.J., 2010. Investigating soil moisture–climate interactions in a changing climate: A review. Earth Sci. Rev. 99 (3–4), 125–161.
Shao, Z., Wu, W., Li, D., 2021. Spatio-temporal-spectral observation model for urban remote sensing. Geo. Spat. Inf. Sci. 24 (3), 372–386.
Sims, D.A., Rahman, A.F., Cordova, V.D., El-Masri, B.Z., Baldocchi, D.D., Bolstad, P.V., Flanagan, L.B., Goldstein, A.H., Hollinger, D.Y., Misson, L., Monson, R.K., Oechel, W. C., Schmid, H.P., Wofsy, S.C., Xu, L., 2008. A new model of gross primary productivity for North American ecosystems based solely on the enhanced vegetation index and land surface temperature from MODIS. Remote Sens. Environ. 112, 1633–1646.
Sitch, S., Friedlingstein, P., Gruber, N., Jones, S.D., Murray-Tortarolo, G., Ahlstrom, A., Doney, S.C., Graven, H., Heinze, C., Huntingford, C., Levis, S., Levy, P.E., Lomas, M., Poulter, B., Viovy, N., Zaehle, S., Zeng, N., Arneth, A., Bonan, G., Myneni, R., 2015. Recent trends and drivers of regional sources and sinks of carbon dioxide. Biogeosciences 12 (3), 653–679.
Smilauer, P., Leps, J., 2014. Multivariate Analysis of Ecological Data Using CANOCO5, 2nd ed. Cambridge University Press, New York.
Sun, Y., Frankenberg, C., Wood, J.D., Schimel, D.S., Jung, M., Guanter, L., Drewry, D.T., Verma, M., Porcar-Castell, A., Griffis, T.J., Gu, L., Magney, T.S., Köhler, P., Evans, B., Yuen, K., 2017. OCO-2 advances photosynthesis observation from space via solar-induced chlorophyll fluorescence. Science 358 (6360) eaam5747.
Ter Braak, C.J., Smilauer, P., 2002. CANOCO reference manual and CanoDraw for Windows user's guide: software for canonical community ordination (version 4.5). https://www.canoco.com.
Ueyama, M., Harazono, Y., Ichii, K., 2010. Satellite-based modeling of the carbon fluxes in mature black spruce forests in Alaska: a synthesis of the eddy covariance data and satellite remote sensing data. Earth Interact. 14 (13), 1–27.
Vergutz, L., Manzoni, S., Porporato, A., Novais, R.F., Jackson, R.B., 2012. Global resorption efficiencies and concentrations of carbon and nutrients in leaves of terrestrial plants. Ecol. Monogr. 82 (2), 205–220.
Walther, G.-R., Post, E., Convey, P., Menzel, A., Parmesan, C., Beebee, T.J.C., Fromentin, J.-M., Hoegh-Guldberg, O., Bairlein, F., 2002. Ecological responses to recent climate change. Nature 416 (6879), 389–395.
Wang, S., Zhang, Y., Ju, W., Chen, J.M., Ciais, P., Cescatti, A., Sardans, J., Janssens, I.A., Wu, M., Berry, J.A., Campbell, E., Fernández-Martínez, M., Alkama, R., Sitch, S., Friedlingstein, P., Smith, W.K., Yuan, W., He, W., Lombardozzi, D., Kauts, M., Zhu, D., Lienert, S., Kato, E., Poulter, B., Sanders, T.G.M., Krüger, I., Wang, R., Zeng, N., Tian, H., Vuichard, N., Jain, A.K., Wiltshire, A., Haverd, V., Goll, D.S., Peñuelas, J., 2020. Recent global decline of CO_2 fertilization effects on vegetation photosynthesis. Science 370 (6522), 1295–1300.
White, M.A., Thornton, P.E., Running, S.W., 1997. A continental phenology model for monitoring vegetation responses to interannual climatic variability. Global Biogeochem. Cy. 11 (2), 217–234.
Williams, L.E., Baeza, P., Vaughn, P., 2012. Midday measurements of leaf water potential and stomatal conductance are highly correlated with daily water use of thompson seedless grapevines. Irrigation Sci. 30 (3), 201–212.
Wu, G.L., Cheng, Z., Alatalo, J.M., Zhao, J., Liu, Y., 2021. Climate warming consistently reduces grassland ecosystem productivity. Earth's Future 9(6), e2020EF001837.
Xu, C., McDowell, N.G., Fisher, R.A., Wei, L., Sevanto, S., Christoffersen, B.O., Weng, E., Middleton, R.S., 2019. Increasing impacts of extreme droughts on vegetation productivity under climate change. Nat. Clim. Change 9 (12), 948–953.
Xu, L., Myneni, R.B., Chapin III, F.S., Callaghan, T.V., Pinzon, J.E., Tucker, C.J., Zhu, Z., Bi, J., Ciais, P., Tømmervik, H., Euskirchen, E.S., Forbes, B.C., Piao, S.L., Anderson, B.T., Ganguly, S., Nemanil, R.R., Goets, S.J., Beck, P.S.A., Bunn, A.G., Cao, C., Stroeve, J.C., 2013. Temperature and vegetation seasonality diminishment over northern lands. Nat. Clim. Change 3 (6), 581–586.
Yue, C., Ciais, P., Houghton, R.A., Nassikas, A.A., 2020. Contribution of land use to the interannual variability of the land carbon cycle. Nat. Commun. 11 (1).
Zeng, X., Hu, Z., Chen, A., Yuan, W., Hou, G., Han, D., Liang, M., Di, K., Cao, R., Luo, D., 2022. The global decline in the sensitivity of vegetation productivity to precipitation from 2001 to 2018. Global Change Biology 28 (22), 6823–6833.
Zhang, Y., Commane, R., Zhou, S., Williams, A.P., Gentine, P., 2020. Light limitation regulates the response of autumn terrestrial carbon uptake to warming. Nat. Clim. Change 10 (8), 739–743.
Zhang, Y., Gentine, P., Luo, X., Lian, X., Liu, Y., Zhou, S., Michalak, A.M., Sun, W., Fisher, J.B., Piao, S., Keenan, T.F., 2022a. Increasing sensitivity of dryland vegetation greenness to precipitation due to rising atmospheric CO2. Nat. Commun. 13, 4875.
Zhang, Y., Piao, S., Sun, Y., Rogers, B.M., Li, X., Lian, X., Liu, Z., Chen, A., Peñuelas, J., 2022b. Future reversal of warming-enhanced vegetation productivity in the Northern Hemisphere. Nat. Clim. Change 12, 581–586.
Zhu, Z., Piao, S., Myneni, R.B., Huang, M., Zeng, Z., Canadell, J.G., Ciais, P., Sitch, S., Friedlingstein, P., Arneth, A., Cao, C., Cheng, L., Kato, E., Koven, C., Li, Y., Lian, X., Liu, Y., Liu, R., Mao, J., Pan, Y., Peng, S., Peñuelas, J., Poulter, B., Pugh, T.A.M., Stocker, B.D., Viovy, N., Wang, X., Wang, Y., Xiao, Z., Yang, H., Zaehle, S., Zeng, N., 2016. Greening of the Earth and its drivers. Nat. Clim. Change 6 (8), 791–795.
Zhuang, Q., Shao, Z., Li, D., Huang, X., Altan, O., Wu, S., Li, Y., 2022a. Isolating the direct and indirect impacts of urbanization on vegetation carbon sequestration capacity in a large oasis city: evidence from Urumqi. China. Geo. Spat. Inf. Sci. 1–13.
Zhuang, Q., Shao, Z., Li, D., Huang, X., Cai, B., Altan, O., Wu, S., 2022b. Unequal weakening of urbanization and soil salinization on vegetation production capacity. Geoderma 411, 115712.